Supporting Information

Ultrafast laser-annealing of perovskite films for efficient perovskite solar cells

*Peng You, Guijun Li, Guanqi Tang, Jiupeng Cao, Feng Yan**

Dr. P. You, Dr. G. J. Li, G. Q. Tang, J. P. Cao, Prof. F. Yan*

Department of Applied Physics, The Hong Kong Polytechnic University, Hung Hom, Kowloon, Hong Kong.
E-mail: apafyan@polyu.edu.hk

Keywords: Perovskite solar cell, laser-annealing, ultrafast, temperature gradient, grain size

Experimental Section

Materials: Methylammonium iodide (MAI), formamidinium iodide (FAI), methylammonium bromide (MABr) and TiO_2 paste (30 NR-D) were ordered from Greatcell Solar Ltd. PbI_2 (99.999%), $PbBr_2$ (99.999%), CsI (99.999%), dimethylformamide (DMF), dimethylsulfoxide (DMSO), chlorobenzene, titanium isopropoxide, methylammonium chloride (MACl), 4-tert-Butylpyridine (tBP) and bis(trifluoromethylsulphonyl)imide lithium salt (Li-TFSI), were all bought from Sigma-Aldrich Ltd. Spiro-OMeTAD was purchased from Lumtec Ltd.

Device fabrication: PSCs were fabricated through a facile solution process with a standard configuration of glass/FTO/compact TiO_2 (c-TiO_2)/mesoporous TiO_2 (mp-TiO_2)/perovskite/spiro-OMeTAD/Au. FTO substrates were firstly cleaned with soap water, ultrasonically cleaned sequentially in acetone, IPA and distilled-water, before drying with air flow. After O_2 plasma treatment for 5 min, a thin c-TiO_2 film (~ 30 nm) was deposited onto the FTO substrates by spin-coating at 4000 rpm from a precursor solution of titanium isopropoxide in anhydrous ethanol (0.15 M, with addition of 1.5 mM HCl from 37 wt.% hydrochloric acid). The as-deposited c-TiO_2 film was annealed

at 80 ºC on hot plate for 10 min and then sintered at 500 ºC for 60 min in air. After cooling down to room temperature, the c-TiO_2 film was coated with a mp-TiO_2 layer (~ 150 nm) on the top at 4000 rpm by using TiO_2 nanoparticle paste (~ 30 nm) diluted in butanol (weight ratio 1:7). After spin-coating, the substrates were dried on hotplate at 100 ºC and then sintered again at 500 ºC for 60 min in air. After cooling down to room temperature, the substrates were immersed in a 40-mM clear aqueous solution of $TiCl_4$ for 30 min at 70 ºC, washed with distilled-water and ethanol sequentially, and sintered again at 500 ºC for 60 min. Finally, after cooling down to 200 ºC, the substrates were transferred into the glovebox (filled with high purity N_2) immediately to deposit perovskite films.

For the preparation of $MAPbI_3$ perovskite films, the perovskite solution was prepared by dissolving 0.5763 g PbI_2 and 0.1986 g MAI in 1 ml mixed solvents of anhydrous DMF and DMSO (volume ratio, 8:1), and was then spin-coated on the mp-TiO_2 films at 4000 rpm for 30 s in the glovebox. After 10 s from the beginning of the spin-coating process, about 100 μl of chlorobenzene was poured onto the spinning substrate. For thermal-annealing processes, the substrates were annealed on a hotplate in the glovebox at 100 ºC for 30 min. For laser-annealing processes, the as-deposited perovskite films were transferred into a dry air chamber (humidity < 5%), where a laser scanning system was built as shown in **Figure S1a**. A continuous-wave laser diode was attached on an X-Y moving system driven by 3 stepper motors. The laser beam was pointing at the vertical direction. The laser scanning track patterns were designed with Autodesk AutoCAD software. The laser beam spot can move on top of the sample surface along the track as shown in **Figure S1b** (the step distance was kept at 0.1 mm when circular beam was used)**.** The laser scan speed can be customized through the software while the laser output power can be tuned through an external voltage source meter. 3 laser diodes (with wavelengths of 405 nm, 450 nm and 660 nm) were used in this work. The laser output power was calibrated with a light intensity power meter every time before experiment. The distance between the laser diode and the sample surface was about 10 cm. When a cylindrical convex lens was placed in the light path of the laser beam, linear laser beam can be obtained. The surface temperature of the perovskite films was monitored with a Fluke Ti400 infrared thermal imager (sensitivity≦0.05 °C). To prepare FAMA mixed perovskite films, the precursor solution was prepared by dissolving 258 mg FAI, 726 mg PbI_2, 13 mg MABr, 44 mg $PbBr_2$, 30 mg MACl in 1ml mixed solvents of DMF and DMSO (volume ratio, 8:1). Then, 80 μl $CsPbI_3$ solution (1 M, also dissolved in DMF and DMSO, 8:1) was added into the FAMA perovskite solution to get the final $(CsPbI_3)_{0.05}(FAPbI_3)_{0.95}(MAPbBr_3)_{0.05}$ (CsFAMA) mixed perovskite solution. After filtering, the mixed perovskite solution was spin-coated onto mp-TiO_2 films at 1000 rpm and 5000 rpm for 5 s and 20 s, respectively. 200 ul ethyl

ether was poured on the spinning substrate after 20 s. For thermal-annealing, the as-deposited mixed perovskite films were annealed at 150 °C for 10 min on hotplate, while the laser-annealing process of mixed perovskite films was the same with that of $MAPbI_3$ perovskite.

After the thermal or laser annealing processes, a spiro-OMeTAD solution (75 mg/ml in chlorobenzene) was spin-coated on the perovskite films at 4000 rpm for 30 s in glovebox. The spiro-OMeTAD solution (1 ml) was doped with 29 μl tBP and 17.5 μl Li-TFSI (520 mg/ml in acetonitrile). The samples were then taken out from the glovebox and kept in dry air (humidity < 5%) for around 10 hours. Finally, gold electrodes (~ 80 nm) were deposited on top through a shadow mask by thermal evaporation at a pressure of ~ 1×10^{-6} Torr. All the devices were encapsulated with epoxy and glass in the glovebox. The active area of the cells was 6 mm^2, except for the large area devices (~ 1.0 cm^2).

Perovskite film characterization: An X-ray diffraction system (Rigaku SmartLab) was used to check the crystal structure and crystallinity of the fabricated perovskite films. The UV-visible absorbance spectra of the perovskite films were measured with a UV-Vis spectrophotometer (UV-2550, Shimadzu). The perovskite films for PL measurements were prepared on glass substrates. Both the steady-state and time-resolved PL measurements of the films were performed by using an Edinburgh FLSP920 fluorescence spectrophotometer. A 636.2-nm laser was used as an excitation light source here (illuminated from the perovskite film side). Both plan-view and cross-sectional SEM images were obtained by a JEOL JSM-6335F field emission SEM. All the samples for SEM observations were coated with an ultra-thin layer of gold before they were put into the microscope.

Device characterization: The *J-V* curves of the PSCs were measured with a Keithley 2420 source meter under standard 1-sun light illumination of 100 mW/cm^2 (Newport 91160 solar simulator, 300 W, equipped with an AM 1.5 filter). The light intensity was calibrated before the *J-V* test by using a standard reference silicon cell. For a standard sweeping cycle, the external applied bias swept from 1.2 V to 0 V (reverse scan) and then returned to 1.2 V (forward scan). Normally, the voltage scan rate was 30 mV/s. And no preconditioning (such as longtime forward bias or light soaking) was applied before all the measurements. The EQE spectra were obtained by using a standard EQE test system (Newport), consisting of a xenon lamp (Oriel 66902, 300 W), a monochrometor (Newport 66902), a Silicon detector (Oriel 76175_71580), and a dual channel power meter (Newport 2931_C). The measurements were performed in DC mode at room temperature. The EQE response from wavelength of 300 nm to 800 nm

was recorded by a computer. The stable power output characteristics were measured at the maximum power point of the PSCs under standard light illumination of 100 mW/cm^2. The steady-state current as a function of time was recorded by a Keithley 2400 source meter, and the stable output efficiency was calculated from the stable current and the bias voltage applied. The EIS measurements of the devices were carried out under light illumination of 100 mW/cm^2 (white light), by using a Zahner Zennium 40630 electrochemical work station. The oscillating voltage was 50 mV and the applied DC bias voltages varied from 0.2 V to 1.0 V. The frequency of the sinusoidal signal changed from 2 MHz to 1 Hz. For device stability measurements, all the devices encapsulated with epoxy and glass were kept in ambient air with the relative humidity of around 30% under dark or light illumination.

Figures

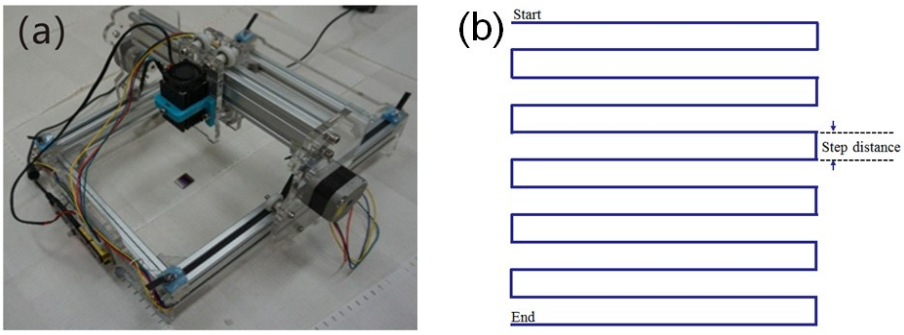

Figure S1. (a) Photograph of the laser-annealing system controlled by a computer. (b) Illustration of the laser scanning track with a fixed step distance.

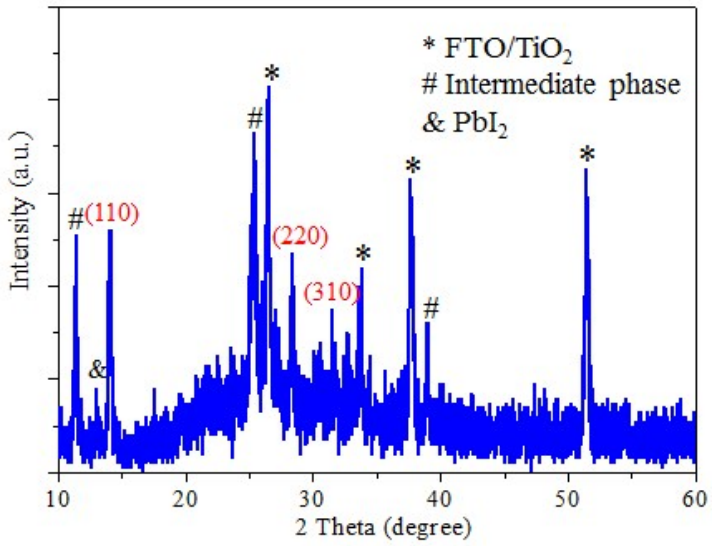

Figure S2. XRD spectrum of the as-deposited $MAPbI_3$ perovskite film, showing (110), (220) and (310) diffraction peaks of tetragonal $MAPbI_3$ perovskite phase.

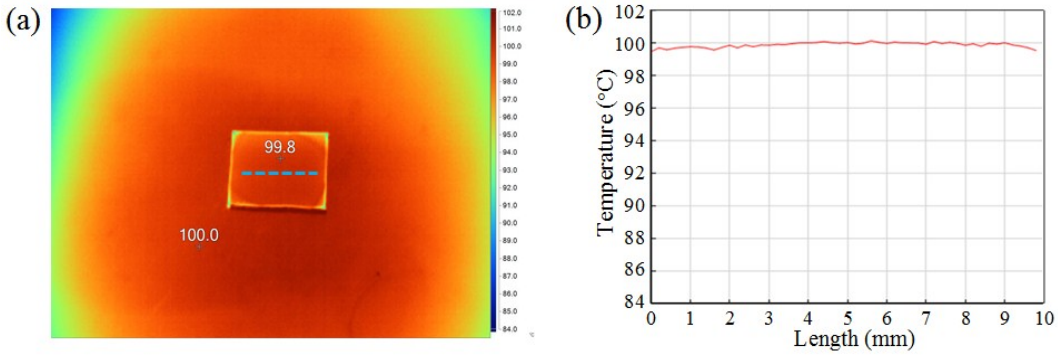

Figure S3. (a) The infrared thermal image of a $MAPbI_3$ perovskite film on a hotplate with a surface temperature of around 100 ºC. (b) The temperature distribution on the sample surface (along the blue line in Figure S3a).

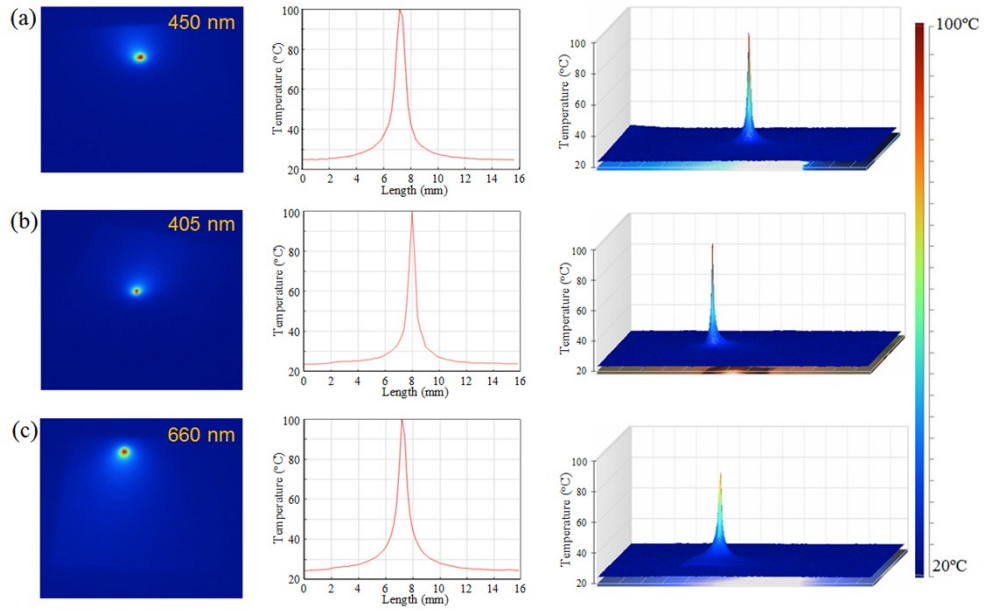

Figure S4. Infrared thermal images of $MAPbI_3$ perovskite films during laser-annealing processes with (a) 450-nm, (b) 405-nm and (c) 660-nm lasers. The laser output power was set as 150 mW for all the lasers.

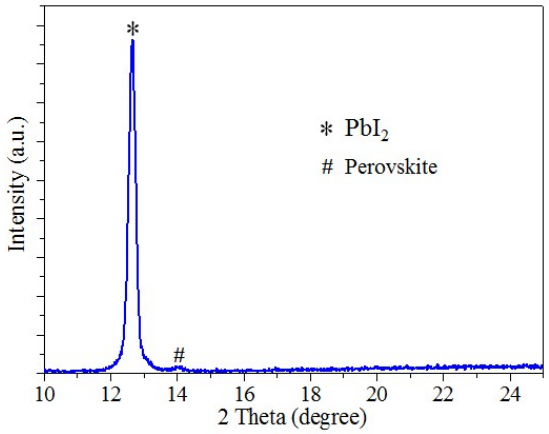

Figure S5. XRD pattern of the decomposed $MAPbI_3$ perovskite film after laser-patterning process by focused laser beam.

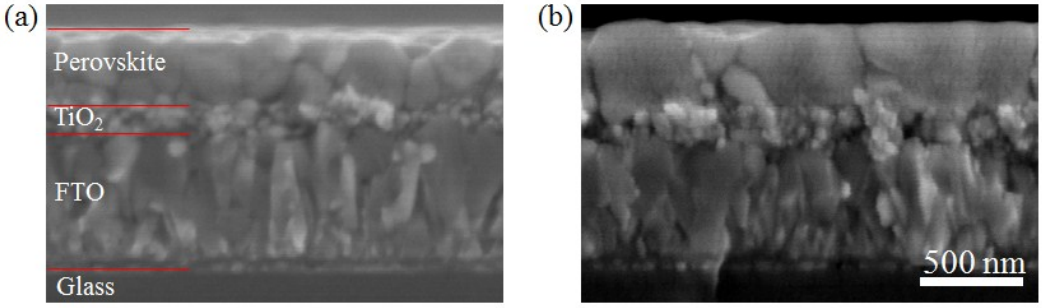

Figure S6. Cross-sectional SEM images of thermal-annealed and laser-annealed $MAPbI_3$ perovskite films on FTO/TiO_2 substrates.

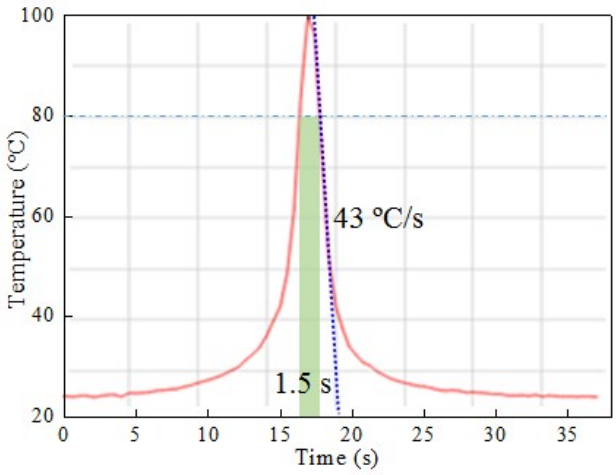

Figure S7. The time dependent temperature of the $MAPbI_3$ perovskite surface under a laser spot with a scanning speed of 25 mm/min. The annealing time above 80 °C is 1.5 s. The surface temperature is increased by laser with the maximum rate of 43 °C/s (slope of the blue dash line).

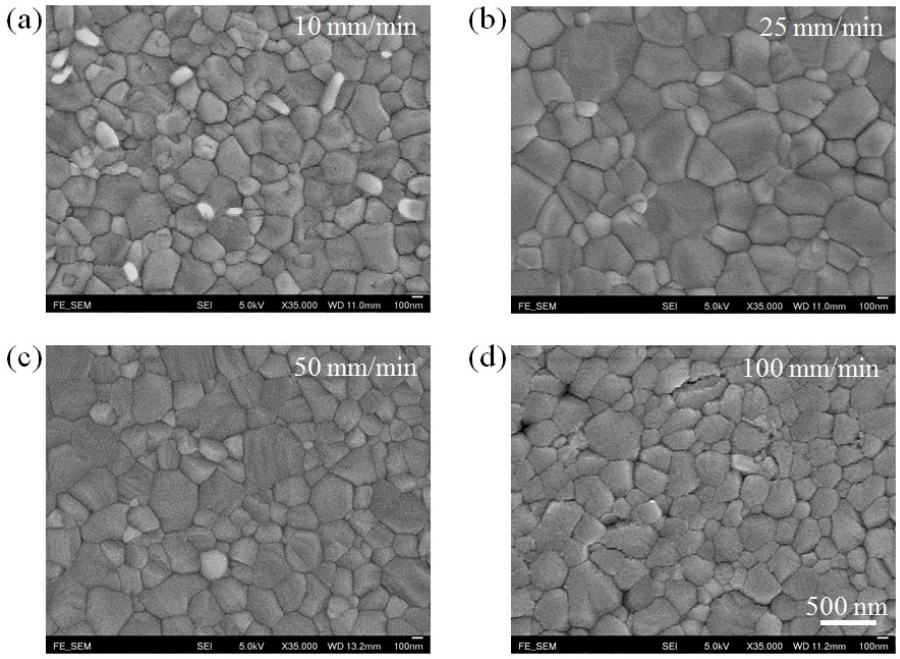

Figure S8. SEM images of $MAPbI_3$ perovskite films fabricated at different laser scanning speeds. 450-nm laser was used, and the laser output power was fixed at 150 mW.

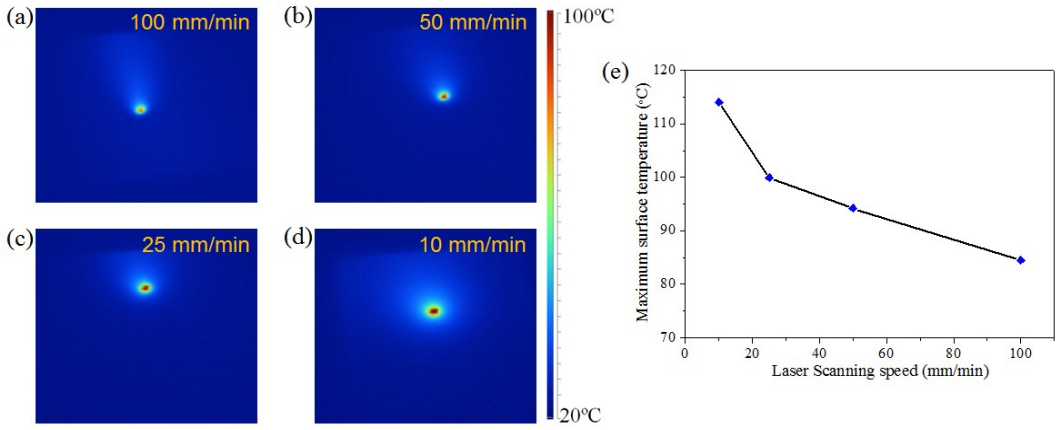

Figure S9. (a-d) The infrared thermal images of $MAPbI_3$ perovskite films during laser-annealing processes with different laser scanning speeds of 100, 50, 25 and 10 mm/min, respectively. (e) The central surface temperatures of the perovskite films derived from the infrared thermal images at different laser scanning speeds.

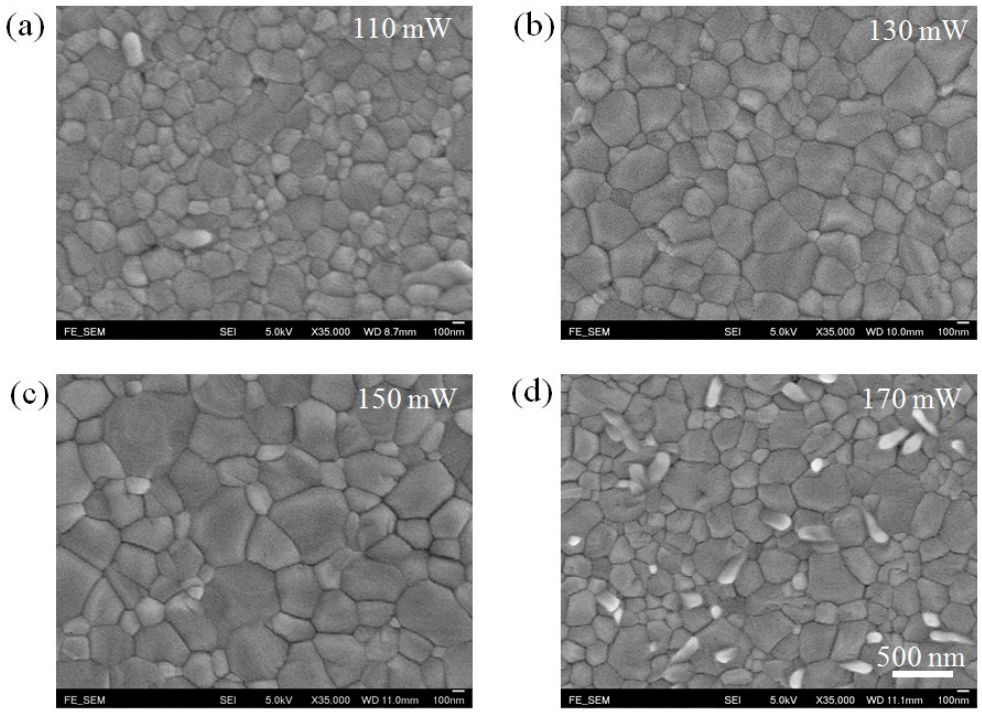

Figure S10. SEM images of $MAPbI_3$ perovskite films fabricated at different laser output power. 450-nm laser was used, and the laser scanning speed was fixed at 25mm/min.

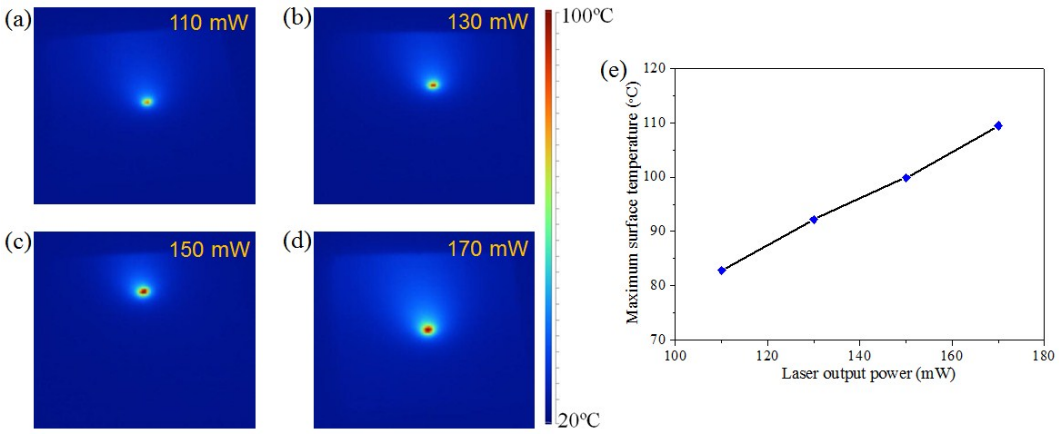

Figure S11. (a-d) The infrared thermal images of $MAPbI_3$ perovskite films during laser-annealing processes with different laser output power of 110, 130, 150 and 170 mW, respectively. (e) The central surface temperatures of the perovskite films derived from the infrared thermal images at different laser output power.

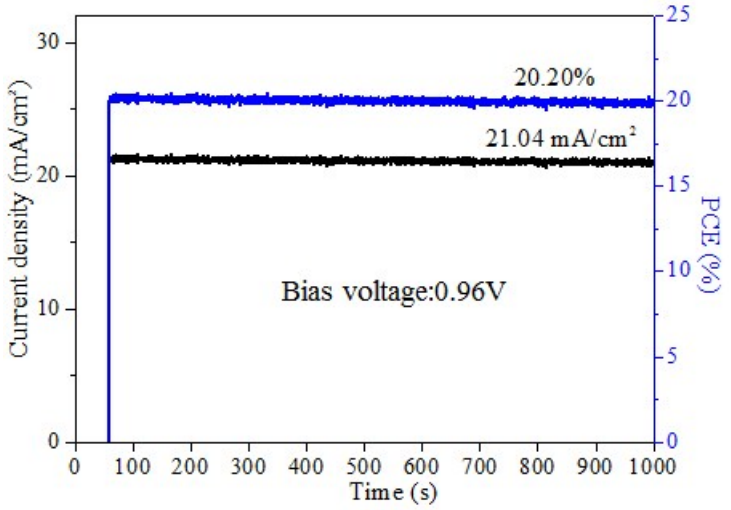

Figure S12. Steady-state photocurrent and efficiency of the best $MAPbI_3$ PSC measured at a bias voltage (0.96 V) at the maximum power point.

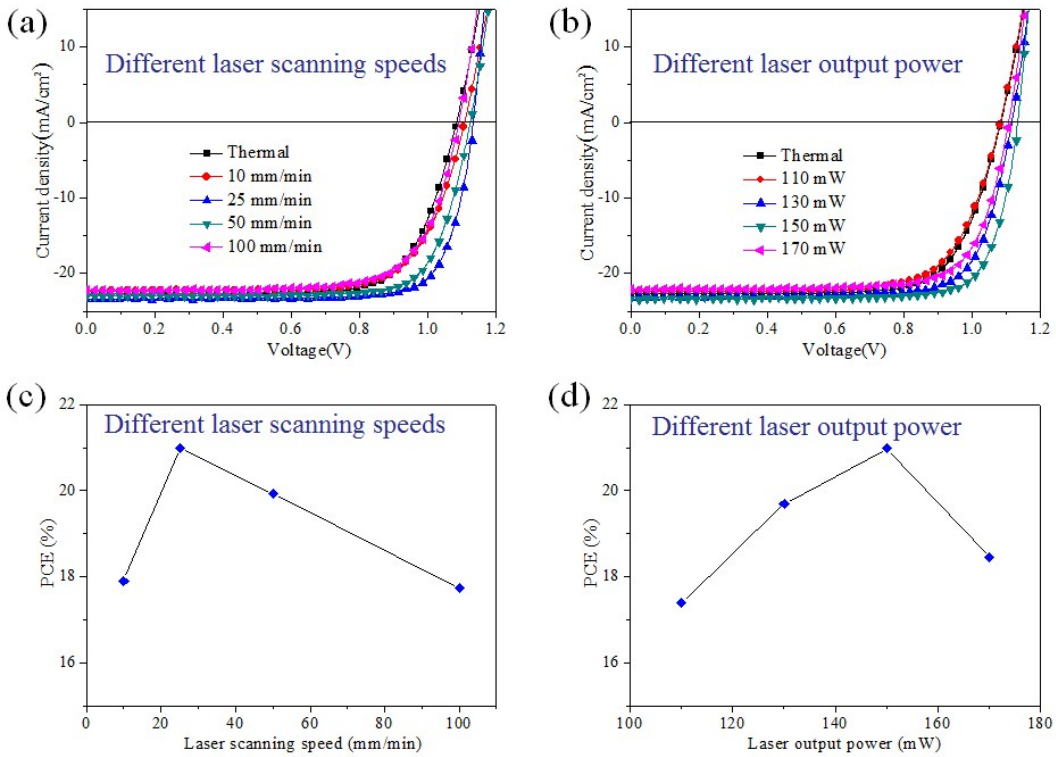

Figure S13. (a) *J-V* characteristics of the $MAPbI_3$ PSCs fabricated at different laser scanning speeds. 450-nm laser was used, and the laser output power was 150 mW. (b) *J-V* characteristics of the $MAPbI_3$ PSCs fabricated at different laser output power. 450-nm laser was used, and the laser scan speed was 25 mm/min. (c) The relationship between the device efficiency and laser scanning speeds. (d) The relationship between the device efficiency and laser output power.

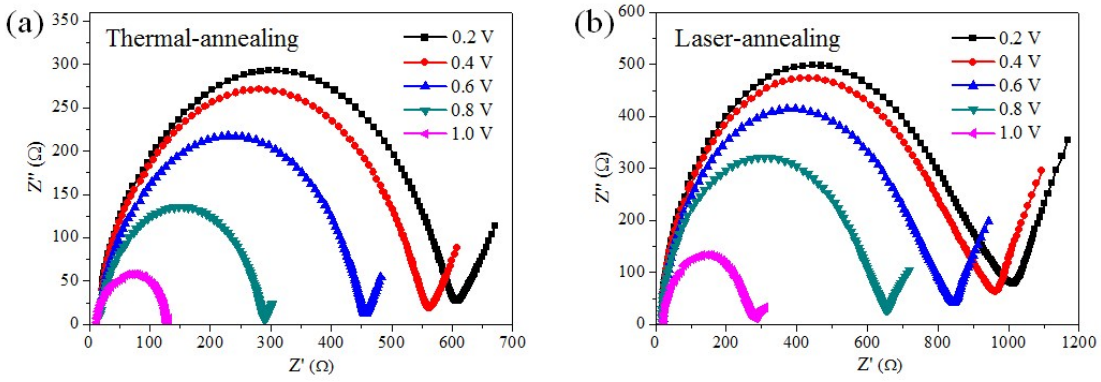

Figure S14. The impedance spectra of $MAPbI_3$ PSCs at different bias voltages under light illumination of 100 mW/cm^2.

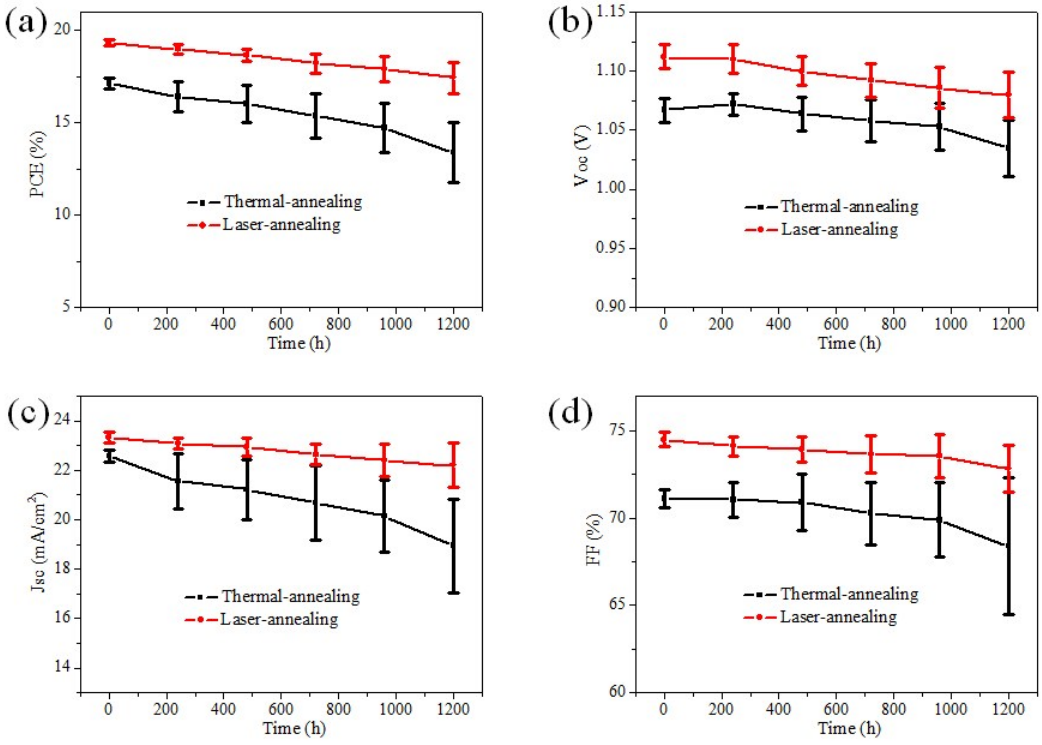

Figure S15. Evolution of the photovoltaic parameters of $MAPbI_3$ PSCs during stability tests (average of 10 devices for each condition). All the devices were encapsulated and kept in air with relative humidity of around 30% (in dark).

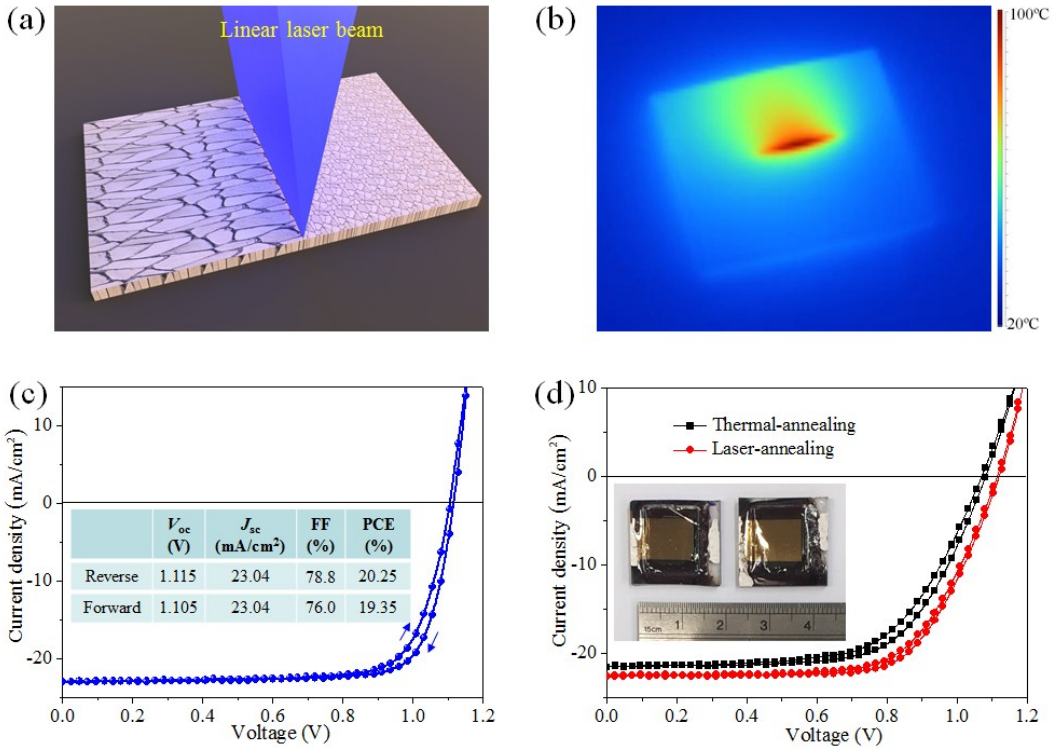

	V_{oc} (V)	J_{sc} (mA/cm^2)	FF (%)	PCE (%)
Reverse	1.115	23.04	78.8	20.25
Forward	1.105	23.04	76.0	19.35

Figure S16. (a) Schematic diagram of the laser-annealing process with a linear laser

beam. (b) Infrared thermal image of the $MAPbI_3$ perovskite film surface during laser scanning process by using a linear laser beam. (c) *J-V* curve of the best $MAPbI_3$ PSC fabricated with the linear laser beam (device area ~ 6 mm^2). (d) *J-V* characteristics of the large-area $MAPbI_3$ PSCs prepared with the linear laser beam (area ~ 1.0 cm^2). Inset shows the photo of the large-area PSCs.

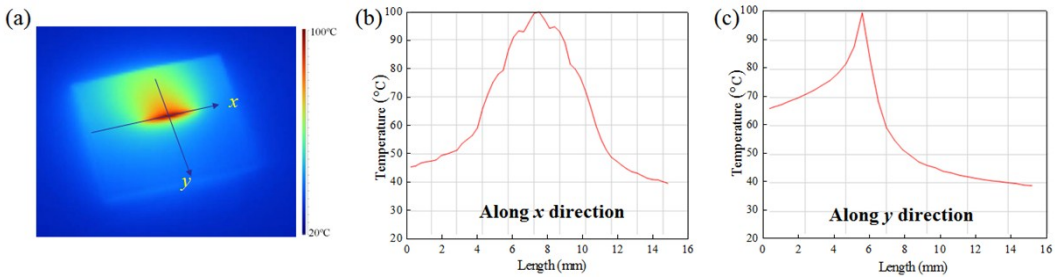

Figure S17. (a) The infrared thermal image of the scanning linear laser beam on the as-deposited $MAPbI_3$ perovskite film. The laser beam was moving along the y axis direction. (b,c) The temperature distribution of the linear laser beam along x and y directions, respectively.

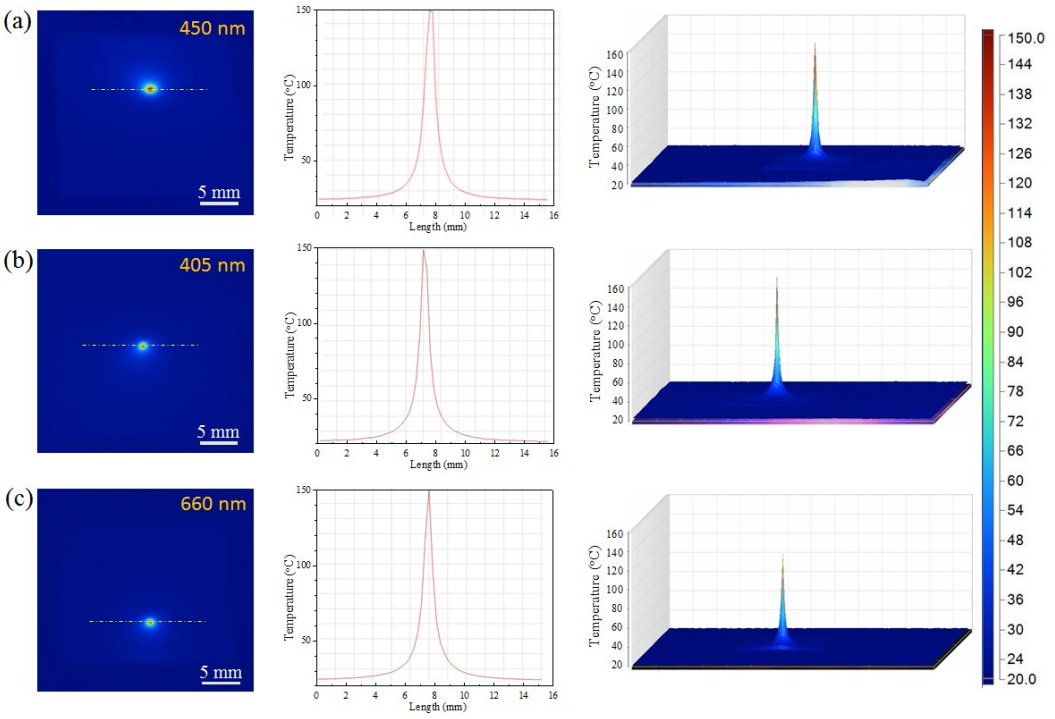

Figure S18. Infrared thermal images of $(CsPbI_3)_{0.05}(FAPbI_3)_{0.95}(MAPbBr_3)_{0.05}$ mixed perovskite films during laser-annealing processes with (a) 450-nm, (b) 405-nm and (c) 660-nm lasers. The laser scanning speed here is 25 mm/min.

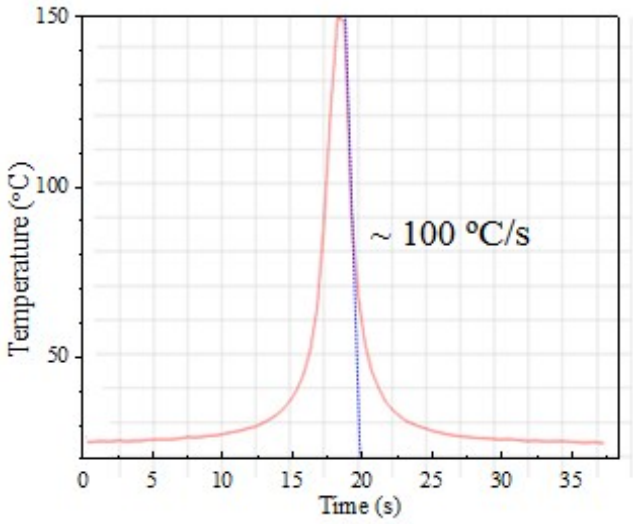

Figure 19. The time-dependent temperature of the mixed perovskite surface under a 450-nm laser spot with a scanning speed of 25 mm/min. The surface temperature is increased by laser with the maximum rate of 100 °C/s (slope of the blue dash line).

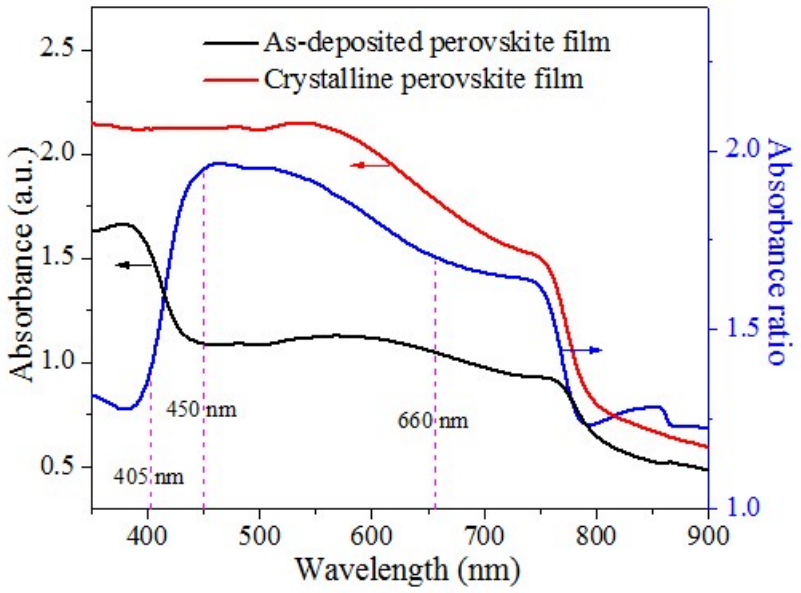

Figure S20. UV-vis absorbance spectra of the as-deposited and laser-annealed mixed perovskite films, along with the absorbance ratio between the two films.

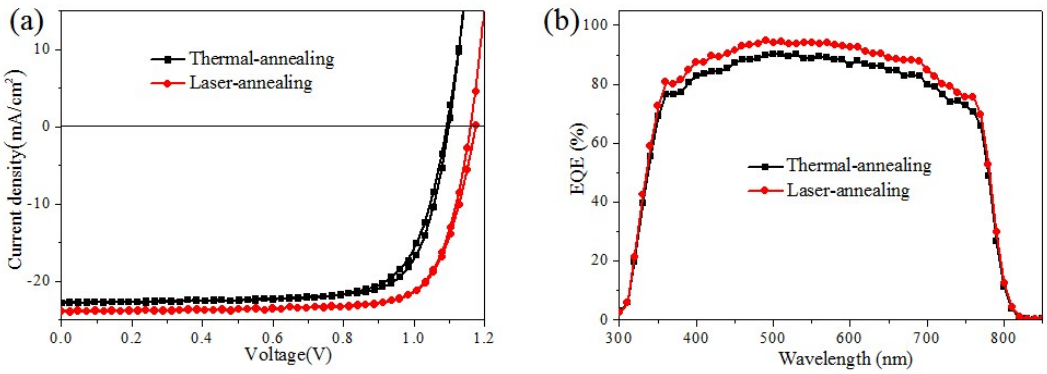

Figure S21. *J-V* characteristics (a) and EQE spectra (b) of the best mixed PSCs fabricated by thermal-annealing and laser-annealing processes.

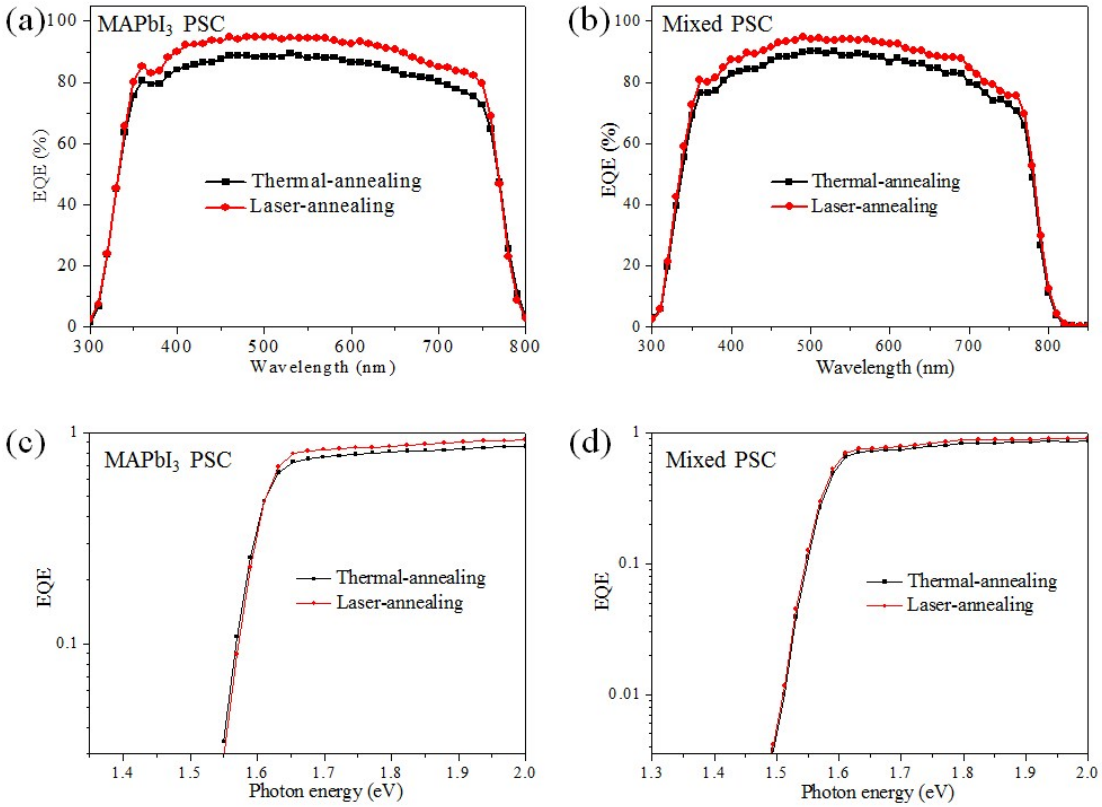

Figure S22. (a,b) EQE spectra of the best $MAPbI_3$ and mixed PSCs. (c,d) Semi-log plot of EQE values versus photon energy.

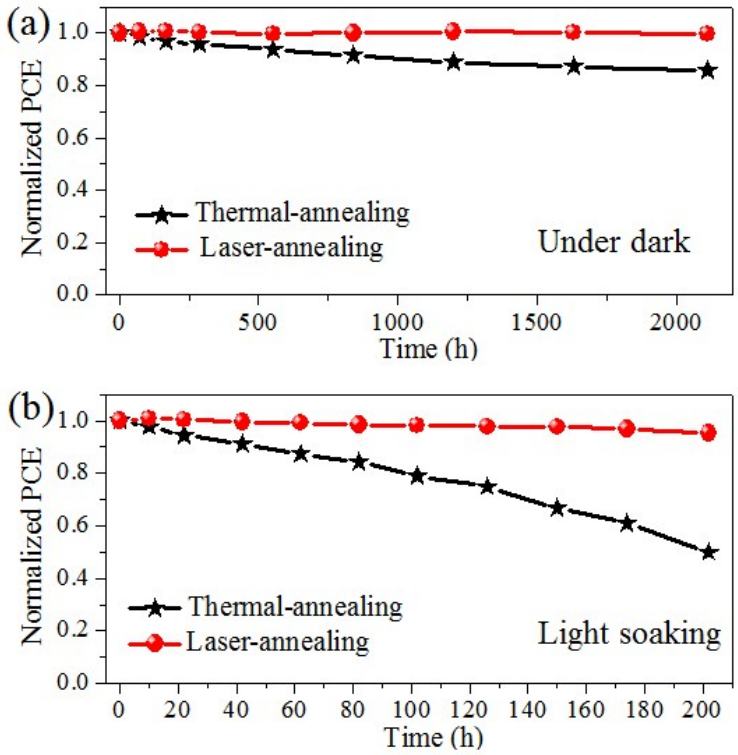

Figure S23. Stability tests of the encapsulated mixed PSCs under dark (a) or under light illumination (b) of 100 mW/cm^2 (AM 1.5G). All the tests were carried out in ambient air with relative humidity around 30%. The device temperature during light soaking is around 40 ºC.

Table S1. The intensity ratio of (110) peak over other diffraction peaks in the XRD spectrum of Figure 1e.

Peak intensity ratio	Thermal-annealing	Laser-annealing
$I_{(110)} / I_{(200)}$	11.95	21.36
$I_{(110)} / I_{(202)}$	13.15	16.61
$I_{(110)} / I_{(310)}$	3.65	5.86
$I_{(110)} / I_{(314)}$	13.84	15.74

Table S2. The average grain size calculated based on SEM images in Figure 2.

Annealing methods	Laser wavelengths	Average grain size (nm)
Thermal-annealing	--	206
Laser-annealing	405 nm	313
	450 nm	476
	660 nm	333

Table S3. Photovoltaic parameters of $MAPbI_3$ PSCs fabricated at different laser scanning speeds. 450-nm laser was used, and the laser output power was 150 mW.

Annealing methods	Laser scanning speed (mm/min)	V_{OC} (V)	J_{SC} (mA/cm^2)	FF (%)	PCE (%)	Champion PCE (%)
Thermal-annealing	--	1.069±0.011	22.36±0.47	70.64±2.02	16.89±0.72	18.10
Laser-annealing	10	1.099±0.011	21.93±0.32	71.21±1.29	17.16±0.41	17.91
	25	1.124±0.009	23.29±0.20	77.27±1.16	20.23±0.35	20.98
	50	1.106±0.011	23.08±0.25	75.85±1.25	19.37±0.43	19.93
	100	1.077±0.011	21.85±0.40	73.08±1.30	17.20±0.38	17.74

Table S4. Photovoltaic parameters of $MAPbI_3$ PSCs fabricated at different laser output power. 450-nm laser was used, and the laser scan speed was 25 mm/min.

Annealing methods	Laser output power (mW)	V_{OC} (V)	J_{SC} (mA/cm^2)	FF (%)	PCE (%)	Champion PCE (%)
Thermal-annealing	--	1.069±0.011	22.36±0.47	70.64±2.02	16.89±0.72	18.10
Laser-annealing	110	1.078±0.011	22.05±0.23	69.76±1.48	16.58±0.43	17.39
	130	1.104±0.013	23.04±0.25	75.15±1.03	19.12±0.41	19.69
	150	1.124±0.009	23.29±0.20	77.27±1.16	20.23±0.35	20.98
	170	1.100±0.011	21.82±0.24	74.12±1.31	17.79±0.50	18.46

Table S5. Photovoltaic parameters of the large-area $MAPbI_3$ PSCs (area: 1.0 cm^2).

Annealing methods	Scan directions	V_{OC} (V)	J_{SC} (mA/cm^2)	FF (%)	PCE (%)
Thermal annealing	Reverse	1.08	21.57	65.1	15.18
	Forward	1.07	21.57	62.2	14.36
Laser annealing	Reverse	1.12	22.60	68.2	17.26
	Forward	1.115	22.60	66.0	16.62

Table S6. The average grain size calculated based on SEM images in Figure 5.

Annealing methods	Laser wavelengths	Average grain size (μm)
Thermal-annealing	--	0.88
Laser-annealing	405 nm	1.38
	450 nm	1.84
	660 nm	1.50

Table S7. Photovoltaic parameters of the best mixed PSCs.

Annealing methods	Scan directions	V_{OC} (V)	J_{SC} (mA/cm^2)	FF (%)	PCE (%)
Thermal annealing	Reverse	1.10	22.80	75.8	19.01
	Forward	1.095	22.80	74.3	18.55
Laser annealing (450-nm laser)	Reverse	1.160	23.85	77.6	21.47
	Forward	1.175	23.85	76.7	21.50

Table S8. The Urbach energy (E_u) values derived from the EQE curves.

Solar cells	Annealing method	E_u (meV)
$MAPbI_3$ PSCs	Thermal-annealing	19.8
	Laser-annealing	18.3
Mixed PSCs	Thermal-annealing	15.7
	Laser-annealing	14.2